

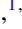




## Information processing in tree networks of excitable elements

Ali Khaledi-Nasab <sup>1,\*,\dagger</sup> Kanishk Chauhan <sup>2,\*,\ddagger</sup> Peter A. Tass <sup>1,\S</sup> and Alexander B. Neiman <sup>2,3,\parallel</sup>

<sup>1</sup>*Department of Neurosurgery, Stanford University, Stanford, California 94305, USA*

<sup>2</sup>*Department of Physics and Astronomy, Ohio University, Athens, Ohio 45701, USA*

<sup>3</sup>*Neuroscience Program, Ohio University, Athens, Ohio 45701, USA*

 (Received 27 July 2020; revised 29 November 2020; accepted 27 December 2020; published 22 January 2021)

We study the collective response of small random tree networks of diffusively coupled excitable elements to stimuli applied to leaf nodes. Such networks model the morphology of certain sensory neurons that possess branched myelinated dendrites with excitable nodes of Ranvier at every branch point and at leaf nodes. Leaf nodes receive random inputs along with a stimulus and initiate action potentials that propagate through the tree. We quantify the collective response registered at the central node using mutual information. We show that in the strong-coupling limit, the statistics of the number of nodes and leaves determines the mutual information. At the same time, the collective response is insensitive to particular node connectivity and distribution of stimulus over leaf nodes. However, for intermediate coupling, the mutual information may strongly depend on the stimulus distribution among leaf nodes. We identify a mechanism behind the competition of leaf nodes that leads to nonmonotonous dependence of mutual information on coupling strength. We show that a localized stimulus given to a tree branch can be occluded by the background firing of unstimulated branches, thus suppressing mutual information. Nonetheless, the mutual information can be enhanced by a proper stimulus localization and tuning of coupling strength.

DOI: [10.1103/PhysRevE.103.012308](https://doi.org/10.1103/PhysRevE.103.012308)

### I. INTRODUCTION

Networks of coupled excitable elements serve as models for a wide range of phenomena such as population dynamics and epidemic spread [1–3], pattern formation in chemical reactions [4,5], and neuronal activity [6,7]. Coupled stochastic excitable systems show a variety of emergent regimes which can be controlled by coupling strength, the network topology and size, or noise strength [8–12].

Tree networks of stochastic excitable units are in use as models of large active dendritic arbors in neurons of the central nervous system [13–15], representing the dendritic network as an excitable medium. Stimuli applied to nodes trigger excitation waves propagating through the tree, resulting in highly nonlinear collective response with extended dynamical ranges [13]. In regular tree networks, propagation of excitations from the central node toward the periphery depends on the branching ratio and the coupling strength. It may fail for branching ratios beyond the critical values [16]. In large tree networks, a combination of bidirectional and unidirectional coupling may form effective loops, leading to self-sustained oscillations [17].

Here we focus on small random tree networks that model certain types of sensory neurons whose dendrites are

myelinated. Examples of such sensory neurons include muscle spindles [18,19], cutaneous mechanoreceptors [20,21], and electroreceptors in paddlefish [22,23]. In such neurons, branches of the dendritic tree are wrapped with myelin, interrupted by the nodes of Ranvier at each branch point, exemplified in Fig. 1. Branching progresses from the primary node (green circle) for a small number (2–5) of generations and terminates at heminodes (red semicircles). The external sensory stimuli generate input currents which are conveyed by thinner neurite processes to heminodes. All nodes, including heminodes, are nodes of Ranvier, the active hot spots of the tree network. Because of the high concentration of  $\text{Na}^+$  channels in nodes, an action potential (AP) can be triggered by a stimulus at any of the heminodes, resulting in several possible spike initiation zones [18,24,25]. APs emerging at multiple heminodes excite nodes in the tree, resulting in a collective response registered at the primary node. Despite the existence of multiple potential spike initiation zones with uncorrelated noise, muscle spindles [25] and paddlefish electroreceptors afferents neurons [26] show coherent periodic spiking.

Myelin decreases the capacitance of and the leak across the dendrite membrane so that a myelinated dendritic arbor can be described by a discrete cable model [28]. In such a model, nodes of Ranvier are connected by passive resistors, leading to a tree network of diffusively coupled excitable units [29,30]. The coupling between units is determined by the geometry of nodes and links and is strong for dendrites with relatively large diameter, such as in muscle spindles and electroreceptors. The latter results in synchronous firing of all nodes in the network, even when peripheral nodes are subjected to uncorrelated noise [29]. Thus, synchronization of

\*These authors contributed equally to this work.

<sup>\dagger</sup>khaledi@stanford.edu

<sup>\ddagger</sup>kanishk.phy@gmail.com

<sup>\S</sup>ptass@stanford.edu

<sup>\parallel</sup>neimana@ohio.edu

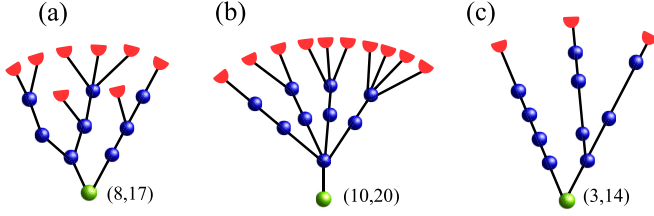


FIG. 1. Examples of tree networks. (a) A muscle spindle afferent from Ref. [27]. (b) An artificial tree with different numbers of heminodes per tree branch. (c) A mechanoreceptor afferent from Ref. [20]. Nodes of Ranvier are shown by circles and semicircles: The primary node is labeled by the green circle, internal nodes are shown by the blue circles, and peripheral nodes (heminodes) are red semicircles. The numbers  $(\mathcal{H}, \mathcal{N})$  next to each tree show the number of heminodes,  $\mathcal{H}$ , and the total number of nodes,  $\mathcal{N}$ .

strongly coupled excitable nodes may serve as a mechanism for coherent spiking observed in muscle spindles and paddlefish electroreceptors afferents mentioned above.

Structure of myelinated terminals, such as the number of nodes, heminodes, and their connectivity, varies among neurons [20,22,27], which may explain the observed population variability of both spontaneous and response dynamics. A model of random trees of coupled identical excitable nodes showed that the tree structure determines the variability of collective firing rate [30]; however, the effect of structural variability on the stimulus response was not studied.

In addition to variability in the tree structure, heterogeneity of stimuli applied to the leaves provides another level of randomness, which is the focus of this paper. The heterogeneity of stimuli to a tree results in distinct responses, which might be an important aspect in sensory information processing and coding because response diversity can be employed on a population level, where outputs of an array of sensory afferents converge to a secondary neuron [21,31]. In touch receptors, for instance, the Merkel-cell neurite complex receives the sensory input and generates an input current to heminodes. Due to the uneven distribution of unmyelinated neurites and Merkel cells across the heminodes, the input to each heminode is nonuniform [20,32]. The loss of Merkel cells also translates into variability in the input to heminodes and may change the receptor sensitivity [33]. Moreover, even the afferents innervating the same end organ might have distinct molecular structure leading to a spatial alignment with differential sensitivity [31].

Heterogeneous stimulation of muscle spindle afferents demonstrates the so-called occlusion, a nonlinear summation, where the response to a combined stimulus applied to two distinct afferent endings is smaller than the sum of individual responses [25,34]. However, a particular mechanism of this effect is still under debate [25,34,35].

Here we characterize the collective response of tree networks of excitable elements to a stimulus using mutual information. Mutual information (MI) is a widely used measure for quantification of the quality of stimulus transmission [36,37]. In our case, MI characterizes the transmission of a stimulus from the periphery of a tree to the primary node. The paper is organized as follows. In Sec. II A we describe a model of Hodgkin-Huxley type nodes coupled on a tree network.

Section II B introduces the mutual information measures for static and time-dependent stimuli. Section III A is devoted to the strong-coupling regime. Effects of coupling strength and heterogeneous stimulus are discussed in Sec. III B, followed up by the conclusion in Sec. IV.

## II. MODEL AND METHODS

Figure 1 exemplifies coupled excitable elements arranged on a tree. Leaf nodes (or heminodes) receive an external stimulus, and the collective response is registered at the primary node.

### A. HH-type model and stimulus

We use the same model as in Ref. [30]. All excitable nodes are identical and governed by a Hodgkin-Huxley (HH) type system. Nodes are diffusively coupled with identical links. Stimulus and noise enter the system via leaf nodes (heminodes). For a tree with  $\mathcal{N}$  nodes and  $\mathcal{H}$  heminodes, the membrane potential of the  $i$ th ( $i = 1, \dots, \mathcal{N}$ ) node is

$$C\dot{V}_i = -I_{\text{ion},i} + \kappa \sum_{j=1}^{\mathcal{N}} A_{i,j}(V_j - V_i) + \delta_{i,l} J_i(t), \quad (1)$$

where  $i = 1$  marks the primary node and  $i = l = \mathcal{N} - \mathcal{H} + 1, \dots, \mathcal{N}$  marks the leaf nodes;  $\kappa$  is the coupling strength;  $C = 2 \mu\text{F}/\text{cm}^2$  is the nodal capacitance, and  $\mathbf{A}$  is the symmetric adjacency matrix that encodes the structure of a tree. Its elements,  $A_{i,j}$ , are either 1 for connected nodes or 0 otherwise.

Ionic current,  $I_{\text{ion},i}$ , across the nodal membrane consists of sodium and leak currents:  $I_{\text{ion},i} = g_{\text{Na}} m_i^3 h_i (V_i - V_{\text{Na}}) + g_L (V_i - V_L)$ , where  $g_{\text{Na}} = 1100 \text{ mS}/\text{cm}^2$  is the maximum sodium conductance,  $V_{\text{Na}} = 50 \text{ mV}$  is the sodium reversal potential,  $g_L = 20 \text{ mS}/\text{cm}^2$  is the leak conductance, and  $V_L = -80 \text{ mV}$  is the leak reversal potential. The gating activation,  $m_i$ , and inactivation,  $h_i$ , variables obey the dynamics

$$\begin{aligned} \dot{m} &= \alpha_m(V)(1 - m) - \beta_m(V)m, \\ \dot{h} &= \alpha_h(V)(1 - h) - \beta_h(V)h, \end{aligned} \quad (2)$$

with the rate functions:

$$\begin{aligned} \alpha_m(V) &= 1.314(V + 20.4)/\{1 - \exp[-(V + 20.4)/10.3]\}, \\ \beta_m(V) &= -0.0608(V + 25.7)/\{1 - \exp[(V + 25.7)/11]\}, \\ \alpha_h(V) &= -0.068(V + 114)/\{1 - \exp[(V + 114)/11]\}, \\ \beta_h(V) &= 2.52/\{1 + \exp[-(V + 31.8)/13.4]\}. \end{aligned}$$

The external current,  $J_i(t)$ , in Eq. (1) is applied to the  $\mathcal{H}$  leaf nodes only, hence the Kronecker delta,  $\delta_{i,l}$ , where the index  $l$  marks leaf nodes. The external current comprises the offset constant current,  $I_0$ , zero mean Gaussian white noise,  $\xi_l(t)$ , and a stimulus  $s(t)$ :

$$J_l(t) = I_0 + \sqrt{2D} \xi_l(t) + \sigma_l s(t), \quad l = \mathcal{N} - \mathcal{H} + 1, \dots, \mathcal{N}, \quad (2)$$

where noise of intensity  $D$  is uncorrelated for different leaf nodes, i.e.,  $\langle \xi_l(t) \xi_k(t + \tau) \rangle = \delta_{l,k} \delta(\tau)$ . In the following for simplicity, we consider a static stimulus,  $s(t) \equiv s$ , where  $s$  is sampled from a Gaussian random distribution with zero mean and unit standard deviation (SD). A set of  $\sigma_l$  weighs the

stimulus applied to leaf nodes and thus models a heterogeneous stimulation of a tree.

In the absence of noise and stimulus,  $D = s = 0$ , the isolated HH node's equilibrium passes through a subcritical Andronov-Hopf bifurcation at  $I_0 = I_{AH} \approx 29.06 \mu\text{A}/\text{cm}^2$ . The corresponding pair of stable and unstable limit cycles disappears at  $I_0 = I_{SN} \approx 28.15 \mu\text{A}/\text{cm}^2$  via the saddle-node bifurcation [29]. For  $I_0 < I_{SN}$  the node is in excitable regime. In the narrow range of  $I_{SN} < I_0 < I_{AH}$ , the single node is bistable with coexisting stable equilibrium and stable limit cycle.

Model equations were integrated numerically using the explicit Euler-Maruyama method with a time step of  $0.1 \mu\text{s}$ .

### B. Collective response and mutual information

We quantified the collective response of a tree network to a stimulus applied to leaf nodes by the MI between the stimulus and the response of the primary node. For the static stimulus used in this study, we used the spike count,  $n(T)$ , as the response of the primary node in a long time window. Spikes generated by a node were counted when the potential of the node crossed a threshold value of 20 mV on its rising phase. Multiple presentations of the stimulus,  $s$ , drawn from the Gaussian distribution generate an ensemble of the spike counts as in Ref. [38]. The collective response of a tree is then characterized by the mutual information [36,38,39],

$$\mathcal{I} = \sum_i \sum_j P(n_i, s_j) \log_2 \left[ \frac{P(n_i, s_j)}{P(n_i)P(s_j)} \right], \quad (3)$$

where  $P(n_i)$  is the probability that spike count attains the value  $n_i$ ,  $P(n_i, s_j)$  is the joint probability that the spike count attains  $n_i$  and the stimulus has the value  $s_j$ , and  $P(s_j)$  is the probability that  $s = s_j$ .

Estimation of MI with Eq. (3) involves the binning of the Gaussian stimulus and demands lengthy simulations [38]. Instead, we used an accurate binning-free nearest-neighbor MI estimator described in Ref. [40] (outlined in Appendix). We estimated the MI from  $K = 1000$  stimulus trials of duration  $T = 5$  s each. For each trial, we set the initial values of the membrane potentials to  $V = -80$  mV, and those of gating variable to random values between 0 and 1. Every trial was preceded by a 0.5-s period for transition to a steady state. For each trial, the static stimulus was sampled from a Gaussian distribution, giving rise to the integer random spike counts of the primary node.

For a long stimulus trial window as used in this study, the discrete random spike count can be approximated by a continuous Gaussian model [38],

$$x = M(s) + \sqrt{Q(s)}\xi, \quad (4)$$

where  $x$  is a continuous analog of the spike count,  $M(s)$  and  $Q(s)$  are the mean and variance of the spike count in response to the stimulus, respectively, and  $\xi$  is the Gaussian noise with mean 0 and a standard deviation of 1. The mean spike count versus stimulus,  $M(s)$ , represents the transfer function of a tree, akin to the so-called f-I curve.

The MI for the Gaussian model is given by [38]

$$\mathcal{I} = \iint ds dx p(s) p(x|s) \log_2 \left[ \frac{p(x|s)}{\int ds' p(s') p(x|s')} \right], \quad (5)$$

where  $p(s)$  is the stimulus probability density

$$p(s) = \frac{1}{\sqrt{2\pi}\sigma^2} e^{-\frac{s^2}{2\sigma^2}},$$

and the conditional probability density,  $p(x|s)$ , is also Gaussian,

$$p(x|s) = \frac{1}{\sqrt{2\pi}Q(s)} e^{-\frac{[x-M(s)]^2}{2Q(s)}}.$$

Eq. (5) can be simplified for the case of small spike count variance to [38,39],

$$\mathcal{I} \approx \frac{1}{\sqrt{8\pi}\sigma^2} \int ds e^{-\frac{s^2}{2\sigma^2}} \log_2 \left[ \frac{\sigma^2 M'^2(s)}{Q(s)} \right], \quad (6)$$

where  $M'(s) = dM(s)/ds$  is the local slope of transfer function and determines the sensitivity of a neuron to stimulus variations. Equation (6) indicates that the MI results from a competition of sensitivity and spike count variance. In the following we use the stimulus-averaged slope of the transfer function,

$$\chi = \frac{1}{\sqrt{2\pi}\sigma^2} \int ds e^{-\frac{s^2}{2\sigma^2}} |M'(s)|, \quad (7)$$

to quantify the sensitivity of tree networks to static stimulus.

We estimated  $M(s)$  and  $Q(s)$  from simulations of tree networks using the stimulation procedure as outlined above, except that the number of stimulus trials was  $K = 100$ , i.e., an order of magnitude less than that for direct MI estimation. Integrals in Eqs. (5)–(7) were evaluated numerically.

In addition to MI, we characterized the temporal coherence of the primary node firing by the coefficient of variation (CV) of corresponding interspike intervals (ISI). Given a sequence of spike times  $\{t_i\}$  within the stimulus windows, the ISI sequence is  $\tau_i = t_{i+1} - t_i$ ,  $i = 1, \dots, n-1$ , where  $n$  is the spike count. For each stimulation window we calculated the CV as the ratio of the ISI standard deviation to the mean ISI,  $\text{CV} = \text{std}(\tau)/\bar{\tau}$ , and then averaged the CV over all stimulus trials.

## III. RESULTS

### A. Strong-coupling limit

In the case of strong coupling,  $\kappa \rightarrow \infty$ , spiking of all nodes is perfectly synchronized and a tree network with a total of  $\mathcal{N}$  nodes and  $\mathcal{H}$  leaf nodes is equivalent to a single node that receives an effective external current,  $I_{\text{eff}}$ , and its dynamics are governed by [29,30]:

$$\begin{aligned} C\dot{V} &= -I_{\text{ion}} + I_{\text{eff}} + \sigma_{\text{eff}} s + \sqrt{2D_{\text{eff}}}\xi(t), \\ I_{\text{eff}} &= \frac{\mathcal{H}}{\mathcal{N}} I_0, \quad \sigma_{\text{eff}} = \frac{\mathcal{H}}{\mathcal{N}} \sigma, \quad D_{\text{eff}} = \frac{\mathcal{H}}{\mathcal{N}^2} D, \end{aligned} \quad (8)$$

where  $I_0$  is the base current,  $\sigma$  is the average stimulus SD, and  $D$  is the noise intensity for the corresponding tree network. That is, the base current and the stimulus SD applied to leaf nodes scale as  $(\mathcal{H}/\mathcal{N})$  and the noise intensity scales as

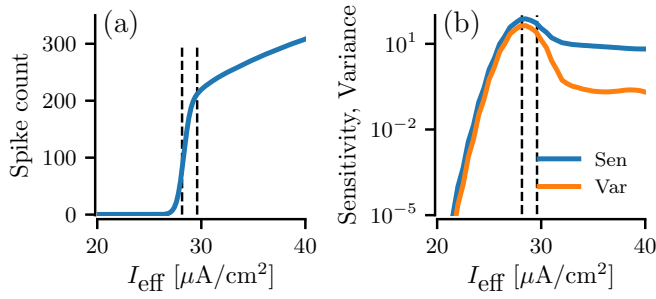


FIG. 2. Response of a single node to static Gaussian stimulus. (a) Mean spike count versus base current. (b) Stimulus-averaged sensitivity (Sen) and spike count variance (Var) versus base current. Units of the sensitivity are  $[\text{spk}/(\mu\text{A}/\text{cm}^2)]$ ; units of spike count variance are  $(\text{spk}^2)$ . The dashed vertical lines show the saddle-node ( $I_{\text{SN}} = 28.15$ ) and Andranov-Hopf ( $I_{\text{AH}} = 29.06$ ) bifurcations for the single HH node. Other parameters are: stimulus SD,  $\sigma_{\text{eff}} = 1 \mu\text{A}/\text{cm}^2$ ; noise intensity  $D_{\text{eff}} = 0.5 (\mu\text{A}/\text{cm}^2)^2 \text{ms}$ .

( $\mathcal{H}/\mathcal{N}^2$ ). Consequently, the collective response of a tree can be predicted from a single node with effective parameters of stimulus and noise. Given the base current, noise intensity, and stimulus, the response is determined by the total number of nodes and leaves, while their particular connectivity and stimulus distribution over leaf nodes are irrelevant [30]. The MI is thus a function of  $\mathcal{H}$ ,  $\mathcal{N}$ , in addition to the external current parameters:  $\mathcal{I}(I_0, D, \sigma; \mathcal{H}, \mathcal{N})$ .

Figure 2 illustrates a single node's response to static stimulus. The mean spike count versus the base current, shown in Fig. 2(a), possesses a sigmoid shape. The slope of this curve is maximal at  $I_0 \approx 28.2 \mu\text{A}/\text{cm}^2$  and corresponds to the saddle-node bifurcation point in the deterministic single-node system. Stimulus-averaged sensitivity Eq. (7) and spike count variance peak at the same value of the base current, Fig. 2(b). This illustrates the fact that, on the one hand, the system becomes most sensitive to a stimulus when poised close to the onset of periodic firing, and on the other hand, high sensitivity to external perturbations implies vulnerability to noise, which is reflected by the maximum of the stimulus-averaged variance of the spike count. The MI shown in Fig. 3 reflects this competition of sensitivity and variability. Initially, MI grows steeply with the increase of base current owing to the increase of sensitivity. The growth of MI is slowed down by the increase of the spike count variance. MI saturates for  $I_0 > 30 \mu\text{A}/\text{cm}^2$ , following saturation of the sensitivity and spike count variability in Fig. 2(b). Figure 3 also demonstrates that the Gaussian model Eq. (4) provides a reliable estimate of the MI (solid line) according to Eq. (5).

Figure 3 also compares the MI estimated from the single node Eq. (8) simulations with the MI estimated for the three trees shown in Fig. 1 for a strong coupling  $\kappa = 500 \text{mS}/\text{cm}^2$ . For such a comparison the parameters of external currents applied to leaf nodes were scaled to yield the same values of the effective single node. For example, tree in Fig. 1(a) (tree a) has  $\mathcal{H} = 8$  leaf nodes and the total  $\mathcal{N} = 17$  nodes. To match the effective node parameters (filled circles in Fig. 3), this tree was simulated with the stimulus SD,  $\sigma_a = (17/8)\sigma_{\text{eff}} = 2.125 \mu\text{A}/\text{cm}^2$ , and noise intensity  $D_a = (\mathcal{N}^2/\mathcal{H})D_{\text{eff}} = 18.0625 (\mu\text{A}/\text{cm}^2)^2 \text{ms}$ .

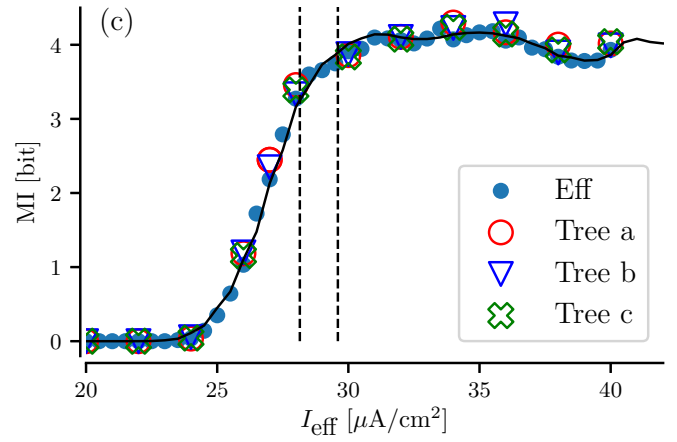


FIG. 3. Mutual information versus base current for the effective single node (Eff) and for the three trees from Fig. 1 (trees a, b, and c) in the strong-coupling limit. Symbols show the direct estimation of MI using nearest-neighbor method [40]; solid line shows Gaussian estimation, Eq. (5). As in Fig. 2, the dashed vertical lines show the saddle-node and Andranov-Hopf bifurcations for the single HH node. Other parameters are as follows: stimulus SD,  $\sigma_{\text{eff}} = 1 \mu\text{A}/\text{cm}^2$ ; noise intensity  $D_{\text{eff}} = 0.5 (\mu\text{A}/\text{cm}^2)^2 \text{ms}$ ;  $\kappa = 500 \text{mS}/\text{cm}^2$ . Values for the number of leaf nodes and total number of nodes for trees a–c are indicated in Fig. 1.

Figure 3 demonstrates an excellent agreement between the direct stimulation of trees and the corresponding strong-coupling approximation. Thus, for strong coupling, the MI can be predicted for an entire ensemble of random trees. As a representative illustration, we consider an example of full binary trees used in Ref. [30]. In such trees, every internal node has two offsprings, while the leaf nodes have none. Given the probability of zero branching,  $p_0$ , and the maximal allowed number of generation,  $G$ , an ensemble of binary trees can be built, e.g., using a Galton-Watson branching process [41,42]. We imposed two additional constraints: (i) the maximum number of generation is 4,  $G = 4$  and (ii) branching extinction is allowed only after the second generation. This results in 13 possible configurations with unique number of leaf nodes and total number of nodes:  $(\mathcal{H}, \mathcal{N}) = (\mathcal{H}, 2\mathcal{H} - 1)$ , where  $\mathcal{H} = 4, 5, \dots, 16$  (see Fig. 4 in Ref. [30]). Note that for this simple example of binary trees, the total number of nodes is fully determined by the number of leaves in a tree,  $\mathcal{N} = 2\mathcal{H} - 1$ . The probability of tree configurations is given by [30],

$$P(\mathcal{H}, p_0) = \left[ \sum_{i=0}^4 \sum_{j=0}^{2i} \delta_{i+j, \mathcal{H}-4} \binom{4}{i} \binom{2i}{j} p_0^{4+i-j} \right] (1 - p_0)^{\mathcal{H}-4}. \quad (9)$$

Instead of fixing parameters of the effective node as was done for Fig. 3, we consider an ensemble of binary trees receiving a given stimulus, base current, and noise. This allows for a comparison of responses versus configuration of tree networks. Given the stimulus SD, base current and noise, the MI can be calculated from the effective single node for each of 13 possible configurations,  $\mathcal{I}(\mathcal{H})$ . For the effective node, the base current and the stimulus SD scale as  $(I_{\text{eff}}, \sigma_{\text{eff}}) = [\mathcal{H}/(2\mathcal{H} - 1)](I_0, \sigma)$ , and noise intensity as

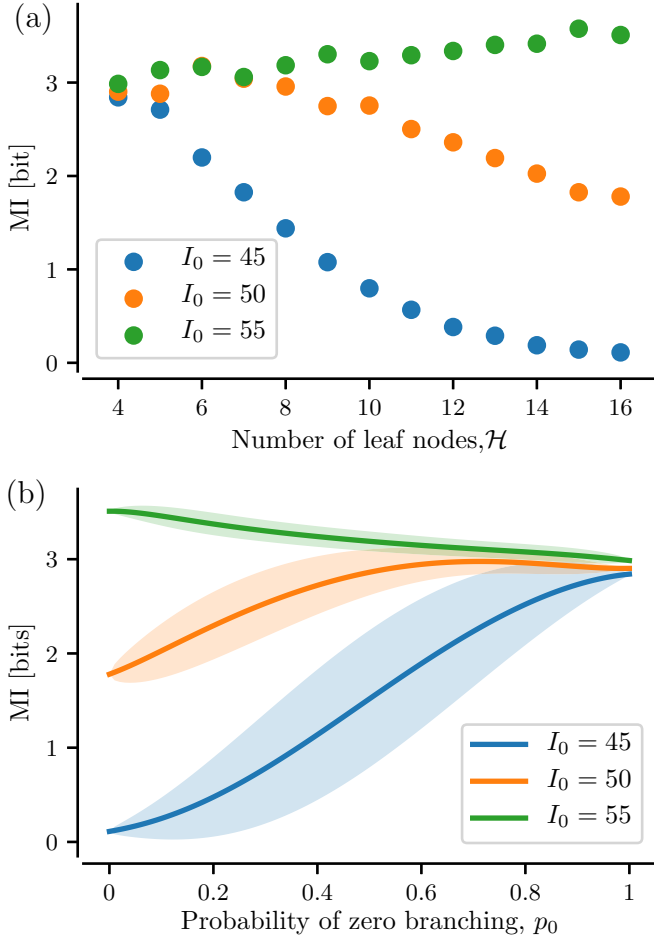


FIG. 4. Mutual information for full binary trees estimated in the strong-coupling limit. (a) MI of 13 possible tree configurations for the indicated values of base current,  $I_0$ . (b) Ensemble average MI versus probability of zero branching,  $p_0$ , for the indicated values of base current,  $I_0$ . The shaded areas show errorbars calculated as  $\langle \mathcal{I} \rangle \pm \sigma_{\mathcal{I}}$ . Other parameters are as follows:  $\sigma = 2 \mu\text{A}/\text{cm}^2$ ,  $D = 50 (\mu\text{A}/\text{cm}^2)^2 \text{ms}$ .

$D_{\text{eff}} = [\mathcal{H}/(2\mathcal{H} - 1)^2]D$ . Further, the ensemble average,  $\langle \mathcal{I} \rangle$ , and the standard deviation,  $\sigma_{\mathcal{I}}$ , are calculated as

$$\begin{aligned} \langle \mathcal{I} \rangle(p_0) &= \sum_{\mathcal{H}=4}^{16} \mathcal{I}(\mathcal{H})P(\mathcal{H}, p_0), \\ \sigma_{\mathcal{I}}^2(p_0) &= \sum_{\mathcal{H}=4}^{16} \mathcal{I}(\mathcal{H})^2 P(\mathcal{H}, p_0) - \langle \mathcal{I} \rangle^2. \end{aligned} \quad (10)$$

The latter measure quantifies the structural variability of responses [30].

Figure 4(a) shows the MI for 13 possible configurations of the considered binary trees and for three values of the base current. The smallest tree with 7 nodes including 4 leaves is characterized by the largest scaling factor,  $\mathcal{H}/(2\mathcal{H} - 1)$ , for the stimulus SD and the base current. The scaling factor decreases for larger trees and is minimal for the largest tree with 16 leaf nodes. Thus, the effective base current, stimulus SD, and noise intensity decrease with the increase of the number of leaf nodes. For  $I_0 = 45 \mu\text{A}/\text{cm}^2$  the corresponding

effective node is in the excitable regime for all possible tree configurations, as the effective base current  $I_{\text{eff}}$  is smaller than the threshold current of the onset of periodic firing,  $I_{\text{SN}} = 28.15 \mu\text{A}/\text{cm}^2$ . For  $I_0 = 50 \mu\text{A}/\text{cm}^2$  the condition  $I_{\text{eff}} < I_{\text{SN}}$  is satisfied for all, but one tree configuration with  $\mathcal{H} = 4$  leaf nodes. Consequently, the firing rate decreases with the increase of tree size, while the coefficient of variation of interspike intervals and the variability of spike count increase [29,30]. Combined with the decrease of effective stimulus SD, this results in the observed decrease of MI. For  $I_0 = 55 \mu\text{A}/\text{cm}^2$ , most of the tree configurations are in the oscillatory regime where a tree fires periodically in the absence of noise and stimulus. In the oscillatory regime, the reduction of the noise intensity,  $D_{\text{eff}} = [\mathcal{H}/(2\mathcal{H} - 1)^2]D$ , for larger trees leads to less variable firing [29], which compensates the reduction of the firing rate and stimulus SD. Consequently, the MI is smaller for the smallest tree and increases slightly toward larger trees.

Figure 4(a) shows bounds of MI for possible tree configurations. For excitable trees, e.g.,  $I_0 = 45 \mu\text{A}/\text{cm}^2$ , the MI can vary from 0.11 to 2.84 bits, while for oscillatory trees  $I_0 = 55 \mu\text{A}/\text{cm}^2$ , the MI range is smaller, from 2.99 to 3.58 bits. Since tree configurations are not equally probable, but follow the probability mass function, Eq. (9), parameterized by the zero branching probability,  $p_0$ , we calculated the ensemble average MI, and its SD according to Eq. (10), shown in Fig. 4(b). The limit of no zero branching,  $p_0 = 0$ , refers to the biggest tree with 16 leaves in the last (fourth) generation and a total of 31 nodes, which occurs with probability  $P(16, 0) = 1$ . The opposite limit,  $p_0 = 1$ , corresponds to the smallest tree with 2 generations only containing 4 leaves and a total of 7 nodes occurring with  $P(4, 1) = 1$  (see Fig. 4 in Ref. [30]). In both these limits, the variability of MI is zero. In the excitable regimes,  $I_0 = 45$  or  $50 \mu\text{A}/\text{cm}^2$ , smaller trees respond more reliably to the stimulus, as shown in Fig. 4(a). Consequently, the ensemble average MI increases with  $p_0$ , as the contribution of smaller trees grows. For larger base currents (e.g.,  $I_0 = 55 \mu\text{A}/\text{cm}^2$ ) the trees are in the oscillatory regime, there is an opposite dependence, where larger trees possess higher MI values. We also note that the variability of MI is larger for excitable trees, consistent with the previous results on the firing statistics [30].

## B. Effect of coupling and heterogeneous stimulus

When the constraint of strong coupling is removed, the response dynamics of a tree depends on the particular connectivity. Trees with the same number of nodes and leaves but different connectivities may show distinct responses that depend on coupling strength, as discussed in Ref. [30]. Besides, a particular arrangement of stimulus becomes important, which we address in this section.

The Gaussian stimulus,  $s$ , with  $\text{SD} = \mathcal{H}\sigma$ , can be applied homogeneously to all leaf nodes, so that each leaf receives the stimulus with the same SD,  $\sigma$ . Alternatively, the stimulus can be distributed heterogeneously amongst leaves such that the total stimulus SD is the same as in the homogeneous case,

$$\mathcal{H}\sigma = \sum_{l=1}^{\mathcal{H}} \sigma_l, \quad l = 1 \dots \mathcal{H}, \quad (11)$$

where  $\sigma_l$  is the stimulus SD for  $l$ th leaf node. In general, one could randomly sample stimulus SDs,  $\sigma_l$ , to obtain equal-sum random variables,  $\sigma_l$ , and then study the variability of responses, as was done in Ref. [43] for the firing rate statistics. The result was that the variability of the firing rate due to stimulus heterogeneity is significant for small and intermediate ranges of coupling strength and vanishes for strong coupling. Here we contrast two limiting cases when the stimulus is applied either homogeneously to all leaf nodes or locally to just one leaf.

We start with the example of a muscle spindle afferent tree of Fig. 1(a). This tree has four generations and three main branches with 2, 3, and 1 leaf nodes (counting left to right) in its peripheral fourth generation. In the homogeneous scenario, the stimulus with the SD,  $\sigma$ , is applied to all  $\mathcal{H} = 8$  leaf nodes of the tree. This can be contrasted to a localized scenario when the stimulus with the entire SD,  $\mathcal{H}\sigma$ , is applied to one of the leaf nodes in a tree branch. Figure 5(a) shows the stimulus averaged firing rate versus coupling strength. No matter how the stimulus is applied, the firing shows almost the same nonmonotonous dependence on the coupling strength: initial increase, a maximum at  $\kappa \approx 1$  mS/cm<sup>2</sup>, and saturation toward a strong-coupling limit value, as discussed in Refs. [29,30]. The stimulus averaged coefficient of variation of interspike intervals (CV) versus coupling strength in Fig. 5(b) shows no significant differences for different stimulation scenarios and follows the dependence discussed in details in Refs. [29,30]. Thus, the temporal coherence of collective firing is similar for homogeneous and localized stimulation.

Contrary to the mean firing rate and CV, the mutual information elucidates distinct responses to homogeneous and localized stimulation, shown in Fig. 5(c). In the case of homogeneous stimulation, the MI initially grows with the coupling strength and saturates for  $\kappa > 1$  mS/cm<sup>2</sup>. For localized stimulation, the dependence of MI versus coupling,  $\kappa$ , becomes nonmonotonous, showing several local extrema. When the stimulus is applied to the branch with one leaf [red curve in Fig. 5(c)], for example, MI shows a local maximum for weak coupling,  $\kappa \approx 1$ . Then the MI drops to almost zero bits at a stronger coupling of  $\kappa \approx 20$ , indicating no stimulus coding in the spike count of the tree's primary node, and then grows again. When the stimulus is applied to the branch with three leaves, MI shows a quite distinct behavior with a single maximum at  $\kappa \approx 20$  mS/cm<sup>2</sup> [green curve in Fig. 5(c)]. Indeed, for strong coupling, the MI converges to its strong-coupling limit for any stimulus configuration. However, for intermediate coupling,  $\kappa = 10$ –60 mS/cm<sup>2</sup>, the collective response of the tree, quantified by MI, is determined by the number of leaf nodes in a branch where the stimulus is applied. The MI is maximal when the stimulus is applied to the branch with three leaves and minimal for stimulation of the single-leaf branch. Stimulating inner leaf nodes, shows responses similar to stimulation of peripheral leaf of the corresponding branch.

We confirmed the observed coupling dependency patterns on a constructed tree, Fig. 1(b). This tree has four branches with one, two, three, and four leaf nodes in the peripheral generation, located at the same distance from the primary node, and no leaves in inner generations. Figure 6 shows qualitatively identical dependency patterns for the stimulus-averaged firing rate, CV, and MI versus coupling as for the

muscle spindle afferent tree (Fig. 5). In the following, we use the constructed tree from Fig. 1(b) to show that the observed distinct responses to localized stimulation can be explained by the competition of stimulated and unstimulated leaf nodes in the process of frequency locking.

Action potentials generated by all leaf nodes contribute to the firing of the primary node. In the homogeneous stimulation case, the firing of all leaves is equally altered by the stimulus and contributes to stimulus encoding in the primary node's spike count. In the localized stimulation, only the stimulated leaf contributes directly to stimulus-related changes in the spike count of the primary node and may compete with unstimulated leaves when the coupling increases. On the one hand, the firing of unstimulated leaves can be altered by the stimulus applied to the stimulated leaf due to the coupling of tree branches through the primary node, tending to increase MI. On the other hand, by the same token, the background firing of unstimulated leaves can alter the firing of the stimulated leaf opposing stimulus-induced variations, thus decreasing MI. We discuss the mechanism behind this behavior further below.

The increase of coupling tends to synchronize the firing of leaf nodes, eventually resulting in synchronous firing of all nodes of the tree [29]. We illustrate this in Fig. 7 by contrasting the firing frequencies of the leaf nodes and the primary node for the homogeneous and localized stimulation. In the case of homogeneous stimulation, Figure 7(a), all leaves receive a stimulus of the same strength, fire at the same rate, and become synchronized for weak coupling. For  $\kappa > 0.3$  mS/cm<sup>2</sup>, the primary node starts to fire being pulled by the leaf nodes. Consequently, the firing frequency of the primary node increases until it becomes locked to the frequency of leaf nodes at  $\kappa \approx 1$  mS/cm<sup>2</sup>, and for larger coupling all nodes of the tree fire at the same rate. In the case of localized stimulation [Figs. 7(b) and 7(c)], the firing rate of the leaf node that receives the entire positive stimulus is higher than that of unstimulated leaf nodes. With the increase of coupling, firing rates of inner nodes, including the primary node, are pulled toward the firing rates of unstimulated leaf nodes and join them at  $\kappa \approx 1.1$  mS/cm<sup>2</sup>. Further increase of coupling pulls these nodes and the stimulated leaf together, and for  $\kappa > 2$  mS/cm<sup>2</sup>, the firing rates of all nodes are locked. Thus, frequency locking of the primary node comes in two main steps: (i) the firing rate of the primary node gets locked to that of the unstimulated leaves and (ii) the firing rates of the unstimulated leaves merge with that of the stimulated node, leading to global synchrony. We note that this is a typical scenario for ensembles of coupled nonidentical oscillators [44,45]. Here the heterogeneity of oscillators is introduced by the stimulus applied to a leaf node.

While Fig. 7 shows frequency locking for a single value of stimulus, a similar picture is obtained for the whole stimulus ensemble by calculating stimulus-averaged firing rates versus coupling. The critical coupling at which stimulus-averaged firing rates of all nodes become locked is  $\kappa_{\text{crit}} = 1.1$  mS/cm<sup>2</sup> for the muscle spindle tree in Fig. 1(a), and  $\kappa_{\text{crit}} = 1.45$  mS/cm<sup>2</sup> for the constructed tree in Fig. 1(b). These values are shown by the vertical dashed lines in Figs. 5 and 6 indicating that MI versus coupling dependencies diverge when the coupling strength exceeds the critical coupling,  $\kappa_{\text{crit}}$ . Once the firing

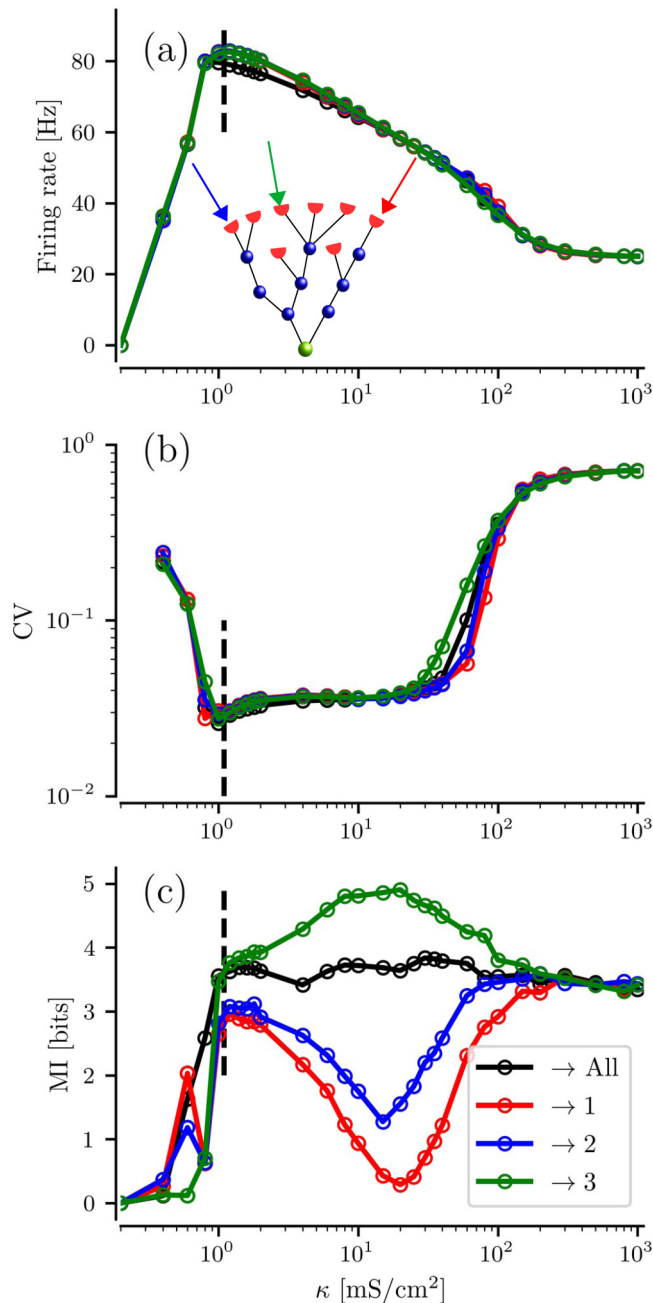


FIG. 5. The collective response of muscle spindle afferent tree to homogeneous and localized stimulation. The inset shows the tree; colored arrows point to the leaf nodes which the stimulus was applied to. (a) Stimulus-averaged firing rate of the primary node versus coupling strength, (b) stimulus averaged CV versus coupling strength, and (c) mutual information versus coupling strength estimated directly using nearest-neighbor method [40]. Line colors correspond to stimulus locations shown in the inset. Black color shows the case of homogeneous stimulation. The dashed vertical lines show the critical coupling,  $\kappa_{\text{crit}} \approx 1.1$   $\text{mS}/\text{cm}^2$ , at which stimulus-averaged firing rates of all nodes are locked. The parameters are as follows:  $I_0 = 60 \mu\text{A}/\text{cm}^2$ ,  $\sigma = 2 \mu\text{A}/\text{cm}^2$ , and  $D = 20 (\mu\text{A}/\text{cm}^2)^2 \text{ms}$ .

rates of all nodes are locked, the stimulated and the unstimulated leaves compete for stimulus-induced changes of their firing as they are connected via the primary node. The longer the average path between stimulated and unstimulated

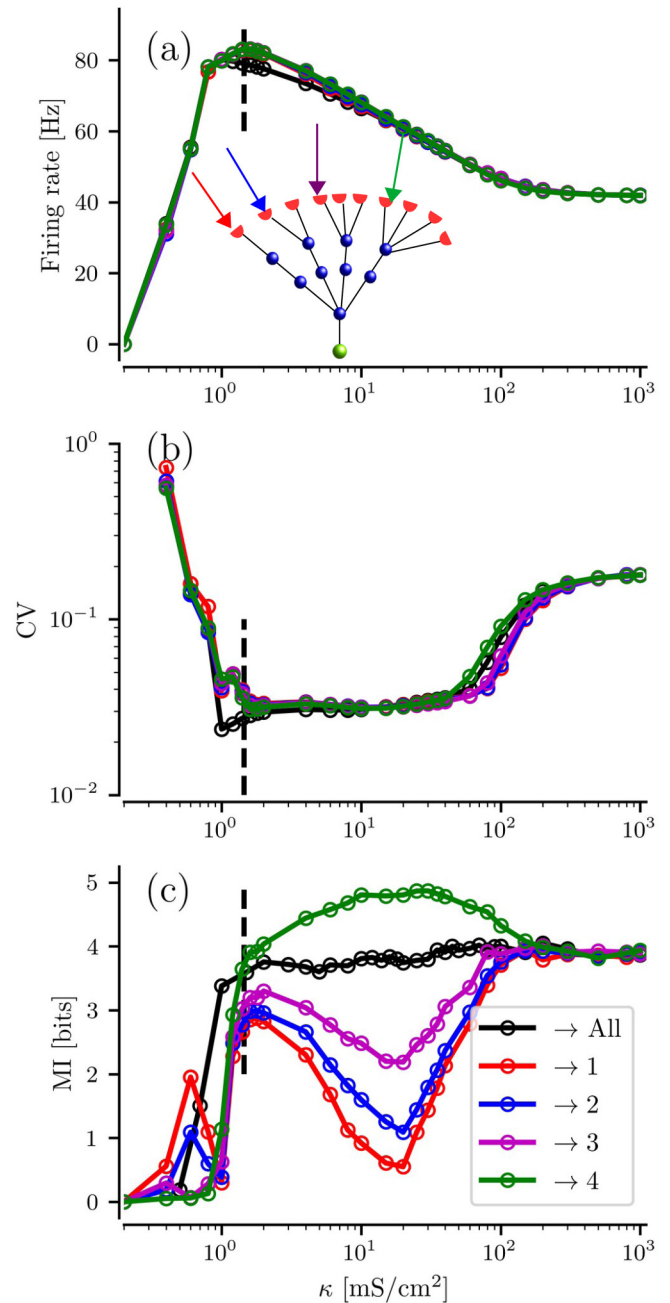


FIG. 6. The collective response of the constructed (artificial) tree to homogeneous and localized stimulation. The inset shows the tree; colored arrows point to the leaf nodes which the stimulus was applied to. Stimulus-averaged firing rate (a), CV (b), and MI (c) versus coupling strength for the constructed tree. Line colors correspond to stimulus locations shown in the inset. Black color shows the case of homogeneous stimulation. The dashed vertical lines show the critical coupling,  $\kappa_{\text{crit}} \approx 1.45$   $\text{mS}/\text{cm}^2$ , at which stimulus-averaged firing rates of all nodes are locked. Other parameters are the same as in Fig. 5.

leaves, the smaller the stimulus' influence on the firing of the unstimulated leaves, and the stronger is the opposition of unstimulated leaves to the stimulus-induced changes in firing of the primary node. The average path between the stimulated leaf and the unstimulated leaves (the average number of links

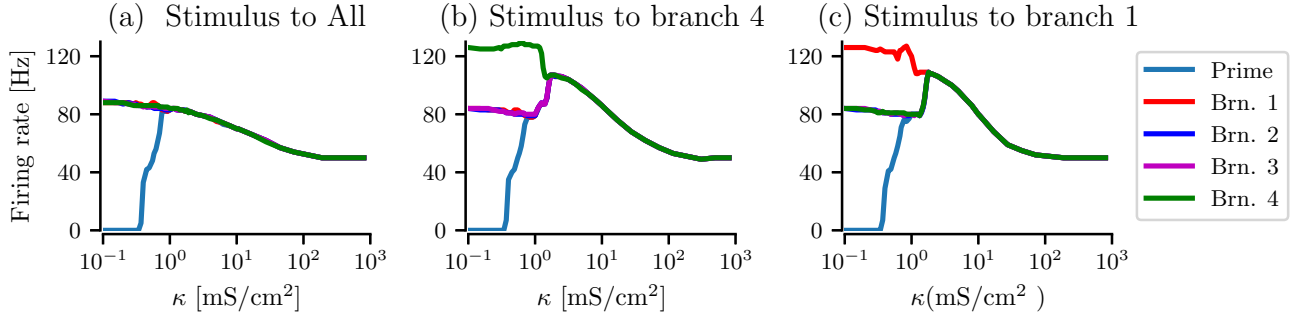


FIG. 7. Frequency locking in the constructed tree shown in Fig. 1(b). The panels show firing rates of the primary node (Prime) and of the leaf nodes from branches with a single leaf (Brn. 1), two leaves (Brn. 2), three leaves (Brn. 3), and four leaves (Brn. 4) versus coupling strength for three stimulation arrangements. (a) Stimulus applied homogeneously to all leaf nodes, (b) localized stimulus to a leaf node in the branch with four leaves (Brn. 4), and (c) localized stimulus to the leaf in the branch with a single leaf (Brn. 1). In all three arrangements the entire stimulus is constant, and equals  $50 \mu\text{A}/\text{cm}^2$ ; in the case of “stimulation to all”, each leaf receives stimulus  $s = 5 \mu\text{A}/\text{cm}^2$ . Other parameters are  $I_0 = 60$  and  $D = 20 (\mu\text{A}/\text{cm}^2)^2 \text{ms}$ .

between stimulated and unstimulated leaves) is longest for the stimulated branch with the single leaf. It decreases with the increase of the number of leaves in the stimulated branch, as several leaves on the stimulated branch are connected by a single link. In particular, for the tree in Fig. 1(b), leaves on different branches are separated by  $L_0 = 6$  links. The average path between a stimulated leaf and all unstimulated leaves is

$$L_b = \frac{(\mathcal{H} - b)L_0 + (b - 1)}{\mathcal{H} - 1},$$

where  $\mathcal{H}$  is the total number of leaves, and  $b$  is the number of leaves on the stimulated branch. For the single-leaf branch,  $L_1 = 6$ , while for the four-leaves branch  $L_4 = 4.333$ . Thus, the stimulation of single-leaf branch results in the strongest resistance of unstimulated leaves to the stimulus, compared to the weakest resistance when the stimulus is applied to the four-leaves branch.

Figure 8 illustrates the effect of the competition of the stimulated and unstimulated leaves on the normalized mean spike count (same as normalized firing rate) of the primary node. For small coupling, Fig. 8(a), the tree responds to all stimulus arrangements. Homogeneous stimulation results in a linear dependence of spike count versus stimulus, while localized stimulation shows rectification owing to the strong stimulus applied to the single leaf. For stronger coupling,

Fig. 8(b), the spike count of the primary node is most affected by the stimulus when it is applied to the four-leaves branch having the shortest average path to unstimulated leaves. In this case, the stimulated branch wins, leading to an increase in MI. On the contrary, when the stimulus is applied to the single-leaf branch, the unstimulated leaves dominate, suppressing changes in the spike count of the primary node due to stimulation [red line in Fig. 8(b)], and resulting in vanishing MI. With further increase of coupling, Fig. 8(c), the tree approaches its strong-coupling limit where responses for different stimulus arrangements eventually coincide.

The described competition mechanism of stimulus encoding is well captured by the stimulus-averaged sensitivity Eq. (7), which is one of the determinants of the mutual information as discussed in Secs. II B and III A. The resistance of the unstimulated leaves to stimulus-related changes in the firing frequency of the primary node flattens the spike count versus stimulus curve,  $M(s)$  [red line in Fig. 8(b)], reduces the slope,  $M'(s)$ , and thus the average sensitivity. Figure 9(a) compares the stimulus-averaged sensitivity for the homogeneous and localized stimulations. For the localized stimulus applied to the single-leaf branch, the sensitivity is at maximum for  $\kappa \approx 1.45 \text{mS}/\text{cm}^2$ , close to the critical coupling of global frequency locking and the MI maximum in Fig. 9(b). Once the frequency-locked state is established, the sensitivity decreases

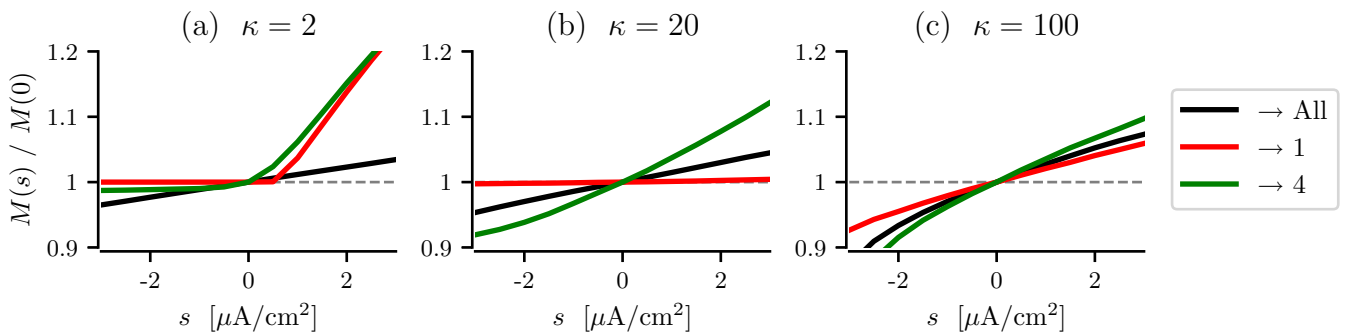


FIG. 8. The normalized spike count of the primary node versus stimulus for the constructed tree shown in Fig. 1(b). The spike count for a given stimulus value,  $M(s)$ , is normalized to the spike count in the absence of stimulus,  $M(0)$ . Each panel shows homogeneous ( $\rightarrow$  All) and two localized stimulation scenarios- the single-leaf branch ( $\rightarrow$  1) and the four-leaves branch ( $\rightarrow$  4). The values of the coupling strength in ( $\text{mS}/\text{cm}^2$ ) are indicated in the panel labels. Other parameters are as follows:  $I_0 = 60 \mu\text{A}/\text{cm}^2$ ,  $D = 20 (\mu\text{A}/\text{cm}^2)^2 \text{ms}$ .



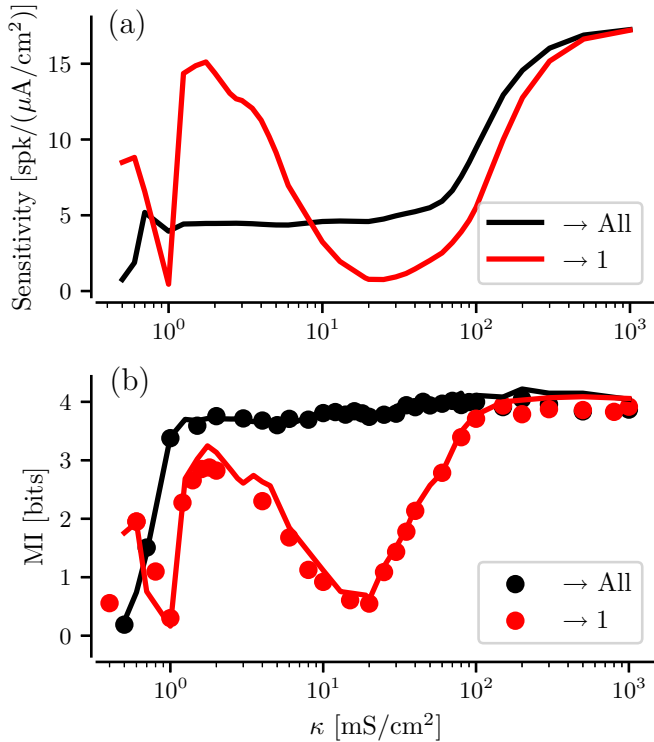


FIG. 9. Average sensitivity (a) and mutual information (b) versus coupling for homogeneous and localized stimulation for the constructed tree from Fig. 1(b). Black color shows the case of homogeneous stimulation ( $\rightarrow$  All). Red refers to the localized stimulation of the branch with a single leaf node ( $\rightarrow$  1). In panel (b), symbols show the direct MI estimation using nearest-neighbor method [40]; solid line shows Gaussian estimation (5). The parameters are as follows:  $I_0 = 60 \mu\text{A}/\text{cm}^2$ ,  $\sigma = 2 \mu\text{A}/\text{cm}^2$ , and  $D = 20 (\mu\text{A}/\text{cm}^2)^2 \text{ms}$ .

with a further increase of coupling, reaching the minimum at  $\kappa \approx 20 \text{ mS}/\text{cm}^2$  and then converges to its strong-coupling limit. Furthermore, the Gaussian model [Eq. (4)] and Gaussian estimate of the mutual information [Eq. (5)] describes the collective response well as illustrated in Fig. 9(b).

The base current,  $I_0$ , and the coupling strength,  $\kappa$ , set the regime of the collective firing of a tree. With the increase of coupling, the entire input to leaf nodes of a tree must be large enough to sustain repetitive firing of the primary node [29,30]. In the deterministic case (no noise or stimulus to leaf nodes), such threshold value of the base current increases with the coupling strength, saturating to the strong-coupling limit value,  $I_\infty = (N/\mathcal{H})I_{\text{th}}$ , where  $I_{\text{th}}$  is a bifurcation value of the single isolated node [30]. For the Hodgkin-Huxley type model used in this study,  $I_{\text{th}}$  corresponds to the saddle-node bifurcation,  $I_{\text{th}} = I_{\text{SN}} \approx 28.15 \mu\text{A}/\text{cm}^2$  [29]. Irregular collective firing characterized by large values of CV occurs for  $I_0 < I_{\text{th}}$  due to noise excitation [29].

Figure 10 compares the sensitivity and MI for homogeneous and localized stimulations for a wide range of the base current and coupling values. In the *homogeneous stimulation case* [Figs. 10(a1) and 10(b1)] the sensitivity is maximal along the line of threshold current versus coupling shown by dashed curves, cf. Fig. 2(b) in Ref. [30]. For a fixed value of coupling,

a local maximum of sensitivity versus base current refers to the transition to repetitive firing [cf. Fig. 2(b)]. If the base current value is large enough to sustain the primary node firing for strong coupling, then the sensitivity versus coupling increases saturating toward its strong-coupling value, as shown in Fig. 9(a), black line. Correspondingly, MI, shown in Fig. 10(b1), increases with coupling and saturates to its strong-coupling value. Otherwise, when the base current is such that the primary node firing vanishes for strong coupling, the sensitivity passes through a maximum and then vanishes, indicated by the black area in the heat map of Fig. 10(a1). In that case, MI also initially increases with coupling, passes through the maximum, and then vanishes.

The heat maps of the sensitivity and MI for the *localized stimulation*, shown in Fig. 10(a2) and 10(b2), clearly demonstrate the distinct response regimes. For strong coupling,  $\kappa > 100 \text{ mS}/\text{cm}^2$ , both the sensitivity and MI show the same dependencies as in the case of homogeneous stimulation. For weak and moderate coupling, the competition of stimulated and unstimulated leaves results in nonmonotonous dependencies of the sensitivity and MI versus coupling strength, resulting in significantly different responses compared to the homogeneous stimulation. In the considered example of localized stimulation, in the intermediate-coupling region of 10–30  $\text{mS}/\text{cm}^2$ , the unstimulated branches of the tree counteract the stimulus and suppress MI for the whole range of base current.

#### IV. CONCLUSION AND DISCUSSION

We have studied the collective response of tree networks of excitable elements to static stimulus. Motivated by the structure of certain sensory neurons whose peripheral dendritic trees are myelinated, we considered a model of small tree networks of diffusively coupled excitable elements. In such a model, excitable elements represent nodes of Ranvier coupled with low-resistant leak-free myelinated links. A stimulus is applied to the leaf nodes, representing the so-called heminodes. Action potentials can be initiated by any heminodes, firing up the inner nodes of Ranvier and, eventually, the primary node. Thus, each leaf node is a potential stimulus encoder, and the collective response is the primary node firing, which we characterized by mutual information.

We used a static Gaussian stimulus within a long time window ( $T = 5 \text{ s}$ ), similar to as in an experimental study on touch receptor afferents [46]. Such a long time window allowed for the large (50–600) number of spikes per stimulus trial, consistent with firing rates of touch receptor afferents [46], paddlefish electroreceptors [23,26], and muscle spindle afferents [25]. The long stimulus window allowed us to use the continuous Gaussian model instead of the computationally expensive direct estimation of MI for parameters screening, such as shown in Fig. 10. The increase or decrease of the stimulus duration did not affect our results qualitatively. In particular the qualitative dependence of the MI versus coupling for different stimulation scenarios, such as shown in Fig. 5(c), is the same for shorter stimulus windows. Furthermore, a time-dependent band-limited Gaussian stimulus gave qualitatively similar results for the upper bound of mutual information rate as for the mutual information in case of static stimulus.

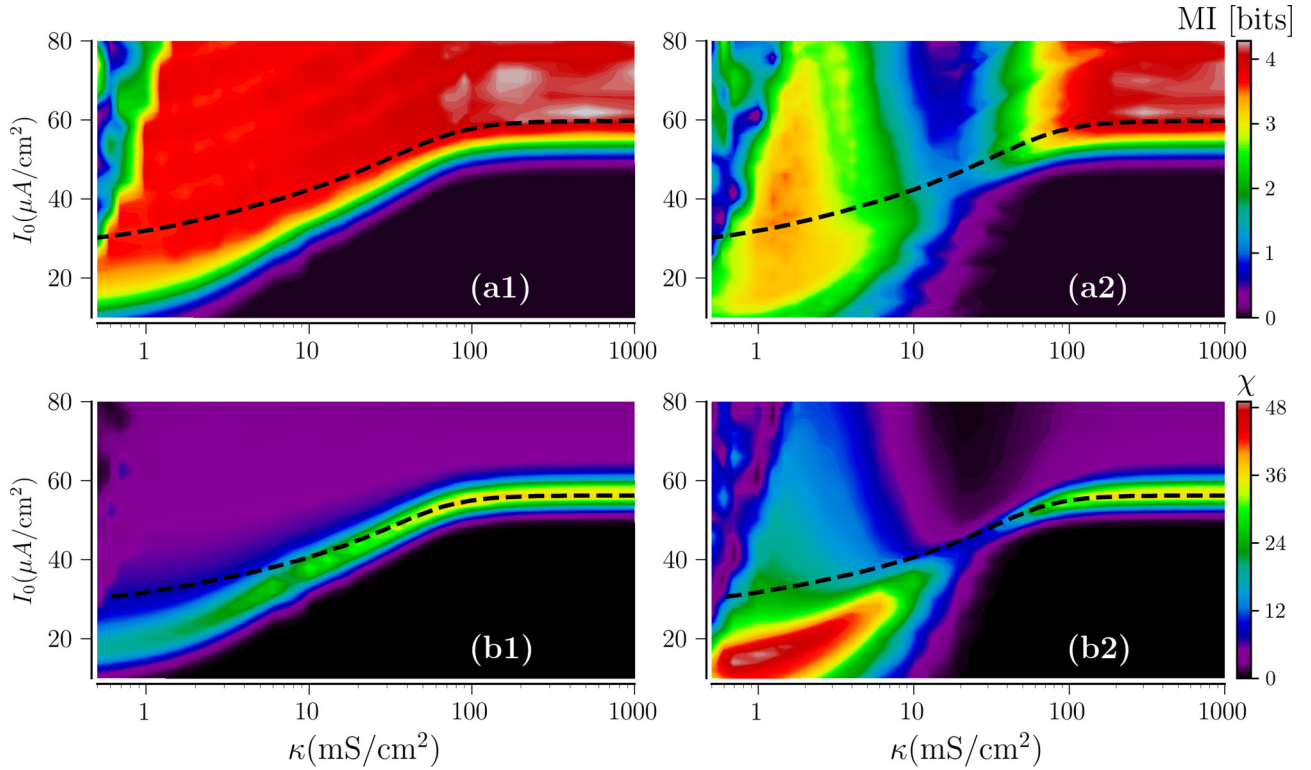


FIG. 10. The average sensitivity and mutual information as functions of the coupling strength,  $\kappa$ , and base current,  $I_0$ , for the constructed tree in Fig. 1(b). Left columns correspond to the homogeneous stimulation and right columns refer to localized stimulation of the branch with a single leaf node. The dashed curves in each panel show the threshold current for the deterministic system, where the primary node starts firing repetitive action potentials; for more on this see Ref. [30]. Panels (a1) and (a2) show the heat map of mutual information, estimated using Gaussian model Eq. (5). Panels (b1) and (b2) show the heat map of average sensitivity  $\chi$  Eq. (7) in units of  $\text{spk}/(\mu\text{A}/\text{cm}^2)$ . Other parameters are the same as in Fig. 9.

The morphology of branched myelinated terminals of sensory neurons, such as in muscle spindle [27,47] and touch receptor [21] afferents, is variable. The underlying random trees are small with one to five generations, and differ in the number of nodes, leaf nodes, branching order, and in node connectivity. This structural randomness may be a source of the observed variability of neuronal firing across a population. Besides, a particular distribution of stimulus over the leaf nodes represents an additional contributor to the observed variability [21].

A previous study [30], showed that the trees' structural randomness results in the variability of the primary node's firing rate across the ensemble. Furthermore, in the physiologically relevant strong-coupling limit [29], the determinant of the firing rate variability is a joint probability distribution of numbers of nodes and leaves in a tree ensemble. In contrast, particular node connectivity does not play a significant role. In this work we quantified the collective response of random trees to external stimuli using mutual information, and examined the effect of stimulus distribution over leaf nodes on collective response.

First, we used the strong-coupling approximation to estimate mutual information between the stimulus applied to leaf nodes of a tree and the firing of the primary node. We showed that mutual information of a tree with a given number of nodes and leaves could be predicted from an effective single node which receives a properly scaled input, irrespective of

particular node connectivity. Using full binary trees as an example, we showed that structural randomness (variation in  $\mathcal{N}$  and  $\mathcal{H}$ ) leads to the variability of mutual information. The extent of the structure-induced variability depends on a particular dynamic regime of a tree, set by the base current. Touch receptors in mice, for example, are characterized by diverse regularity of their discharges: some fire regularly, characterized by small coefficient of variation,  $\text{CV} \approx 0.2$ , while others fire randomly with  $\text{CV} \approx 0.8$  [46]. Regular neurons are likely operating in the oscillatory regime, while irregular neurons are operating in the excitable regime. We showed that while the response of oscillatory trees depends weakly on their particular structure, excitable trees show a wide range of responses, quantified by mutual information. This structure-induced diversity may lead to improved information coding on the level of population, when a large number of primary sensory neurons converge to a secondary neuron [48,49]. Thus, even though individual primary afferents may not be tuned for the optimal information coding, a population (an ensemble of random trees in our case) response benefits from the response diversity of individual sensors, as suggested for touch receptors [21,31].

Second, for a finite coupling strength, we showed that a heterogeneous stimulus distribution over leaf nodes becomes important: A tree with a given topology may show diverse responses when the stimulus is applied to leaves on different branches. This leads to stimulus-heterogeneity-induced

variability of responses, as in touch receptor afferents [20]. Here we studied homogeneous versus localized stimulation and showed that the fate of collective response is determined by the synchronization-induced competition between the stimulated and the unstimulated branches of a tree.

A tree network where leaf nodes receive inputs and generate periodic firing can be viewed as a system of oscillators coupled via excitable media of inner nodes [45]. With the increase of coupling strength, the firing of leaf nodes gets synchronized due to communications via inner nodes. Although a route to synchronization can be quite complicated, involving various high-order mode-locking between leaf nodes and primary node [43,45], for large-enough coupling, all nodes in the tree are frequency locked, eventually. Then, leaf nodes on the unstimulated branch compete with those on the stimulated branch, resisting the stimulus-induced variations, resulting in nonmonotonous dependence of mutual information versus coupling strength. The winner is determined by the shortest average path between stimulated and unstimulated leaves. Thus, mutual information can be enhanced by a proper stimulus localization, e.g., on a branch with the largest number of leaves, compared to homogeneous stimulation. Otherwise, when a branch with a small number of leaves is stimulated, background firing of unstimulated branches may win, obstructing stimulus-induced variations of the primary node firing, and thus, suppressing the mutual information. We note that the effect of stimulus coding degradation due to frequency locking was observed in a P-type electroreceptor model, where the firing of sensory neurons is locked to a higher frequency periodic signal [50]. An interesting question of discrimination between stimuli applied to different branches based on the primary node response requires further study.

Our results are related to the so-called phenomenon of occlusion observed in muscle spindle afferents [25,34,35,51,52]. In these studies, branched myelinated sensory neurons were subjected to distinct stimuli administered to different branches, with the firing of one masking (or occluding) that of

the other. Our results support a model in which the occlusion was attributed to competitive interactions of encoding sites separated by long enough conduction path [25].

Finally, we note that we confirmed the results using other models of excitable nodes such as FitzHugh-Nagumo and Frankenhaeuser-Huxley model for the nodes of Ranvier [29,53].

#### ACKNOWLEDGMENT

A.K.N. and A.N. thank Lutz Schimansky-Geier and Benjamin Lindner for insightful discussions. K.C. and A.N. acknowledge support from the Quantitative Biology Institute and Neuroscience Program at Ohio University.

#### APPENDIX: NEAREST-NEIGHBOR ESTIMATOR OF MUTUAL INFORMATION

We used a nonparametric estimator of mutual information between the discrete variable  $x$  (spike count) and continuous variable  $y$  (stimulus) [40]. Instead of binning of continuous variable, we used the binning-free nearest-neighbor method. Given a set of  $N$  data points,  $(x_i, y_i)$ , the discrete variable  $x$  can have repeated values, while the continuous variable  $y$  cannot, and thus, several values of  $y$  may correspond to one value of  $x$ . For each point of the continuous variable,  $y_i$ , the estimator first looks at the corresponding  $x$  value and extracts the  $N_{x_i}$  data points which all have that same  $x$  value. Then, the estimator locates the nearest neighbor of  $y_i$  among the extracted data points and computes the distance,  $d$ , between  $y_i$  and its nearest neighbor. Then, it counts the number of neighbors,  $m_i$ , of  $y_i$  which lie within distance  $d$  in the full data set. The MI is estimated using [40]

$$\mathcal{I} = \psi(N) - \langle \psi(N_{x_i}) \rangle + \psi(1) - \langle \psi(m_i) \rangle, \quad (\text{A1})$$

where  $\psi(z) = \Gamma'(z)/\Gamma(z)$  is the digamma function, and the averaging is over all data points.

- 
- [1] I. Farkas, D. Helbing, and T. Vicsek, Social behavior: Mexican waves in an excitable medium, *Nature* **419**, 131 (2002).
  - [2] S. P. Borgatti, A. Mehra, D. J. Brass, and G. Labianca, Network analysis in the social sciences, *Science* **323**, 892 (2009).
  - [3] M. E. Newman, Spread of epidemic disease on networks, *Phys. Rev. E* **66**, 016128 (2002).
  - [4] I. Z. Kiss and J. L. Hudson, Chemical complexity: Spontaneous and engineered structures, *AIChE J.* **49**, 2234 (2003).
  - [5] A. S. Mikhailov and G. Ertl, *Engineering of Chemical Complexity* (World Scientific, Singapore, 2012).
  - [6] E. Bullmore and O. Sporns, Complex brain networks: Graph theoretical analysis of structural and functional systems, *Nat. Rev. Neurosci.* **10**, 186 (2009).
  - [7] M. London and M. Häusser, Dendritic computation, *Annu. Rev. Neurosci.* **28**, 503 (2005).
  - [8] B. Lindner, J. Garcia-Ojalvo, A. Neiman, and L. Schimansky-Geier, Effects of noise in excitable systems, *Phys. Rep.* **392**, 321 (2004).
  - [9] R. Toral, C. Mirasso, and J. Gunton, System size coherence resonance in coupled fitzhugh-nagumo models, *Europhys. Lett.* **61**, 162 (2003).
  - [10] M. Gosak, D. Korošak, and M. Marhl, Optimal network configuration for maximal coherence resonance in excitable systems, *Phys. Rev. E* **81**, 056104 (2010).
  - [11] M. Perc, Spatial coherence resonance in excitable media, *Phys. Rev. E* **72**, 016207 (2005).
  - [12] X. Sun, M. Perc, Q. Lu, and J. Kurths, Spatial coherence resonance on diffusive and small-world networks of hodgkin-huxley neurons, *Chaos* **18**, 023102 (2008).
  - [13] L. L. Gollo, O. Kinouchi, and M. Copelli, Active dendrites enhance neuronal dynamic range, *PLoS Comput. Biol.* **5**, e1000402 (2009).
  - [14] L. L. Gollo, O. Kinouchi, and M. Copelli, Statistical physics approach to dendritic computation: The excitable-wave mean-field approximation, *Phys. Rev. E* **85**, 011911 (2012).
  - [15] L. L. Gollo, O. Kinouchi, and M. Copelli, Single-neuron criticality optimizes analog dendritic computation, *Sci. Rep.* **3**, 3222 (2013).
  - [16] N. E. Kouvaris, T. Isele, A. S. Mikhailov, and E. Schöll, Propagation failure of excitation waves on trees and random networks, *Europhys. Lett.* **106**, 68001 (2014).

- [17] L.-S. Zhang, N.-Y. Cui, J.-Z. Zhang, Z.-Y. Zhang, and G. Hu, Self-sustained oscillations in excitable tree networks, *Int. J. Mod. Phys. C* **29**, 1850102 (2018).
- [18] D. Quick, W. R. Kennedy, and R. Poppele, Anatomical evidence for multiple sources of action potentials in the afferent fibers of muscle spindles, *Neurosci.* **5**, 109 (1980).
- [19] G. S. Bewick and R. W. Banks, Mechanotransduction in the muscle spindle, *Eur. J. Physiol.* **467**, 175 (2015).
- [20] D. R. Lesniak, K. L. Marshall, S. A. Wellnitz, B. A. Jenkins, Y. Baba, M. N. Rasband, G. J. Gerling, and E. A. Lumpkin, Computation identifies structural features that govern neuronal firing properties in slowly adapting touch receptors, *Elife* **3**, e01488 (2014).
- [21] K. L. Marshall, R. C. Clary, Y. Baba, R. L. Orłowski, G. J. Gerling, and E. A. Lumpkin, Touch receptors undergo rapid remodeling in healthy skin, *Cell Rep.* **17**, 1719 (2016).
- [22] D. F. Russell, D. E. Rogers, and L. L. Neiman, Nonbinary branching of myelinated dendrites at nodal networks on afferent terminal arbors in paddlefish electroreceptors, *Matters* **5**, e201812000003 (2019).
- [23] D. F. Russell, T. C. Warnock, W. Zhang, D. E. Rogers, and L. L. Neiman, Large-scale convergence of receptor cell arrays onto afferent terminal arbors in the lorenzian electroreceptors of polyodon, *Front. Neuroanat.* **14** (2020).
- [24] J. P. Eagles and R. L. Purple, Afferent fibers with multiple encoding sites, *Brain Res.* **77**, 187 (1974).
- [25] R. Banks, M. Hulliger, K. Scheepstra, and E. Otten, Pacemaker activity in a sensory ending with multiple encoding sites: The cat muscle spindle primary ending, *J. Physiol.* **498**, 177 (1997).
- [26] A. B. Neiman and D. F. Russell, Two distinct types of noisy oscillators in electroreceptors of paddlefish, *J. Neurophysiol.* **92**, 492 (2004).
- [27] R. W. Banks, D. Barker, and M. Stacey, Form and distribution of sensory terminals in cat hindlimb muscle spindles, *Philos. Trans. R. Soc. Lond. B* **299**, 329 (1982).
- [28] G. B. Ermentrout and D. H. Terman, *Mathematical Foundations of Neuroscience* (Springer Science & Business Media, New York, 2010), Vol. 35.
- [29] J. Kromer, A. Khaledi-Nasab, L. Schimansky-Geier, and A. B. Neiman, Emergent stochastic oscillations and signal detection in tree networks of excitable elements, *Sci. Rep.* **7**, 3956 (2017).
- [30] A. Khaledi-Nasab, J. A. Kromer, L. Schimansky-Geier, and A. B. Neiman, Variability of collective dynamics in random tree networks of strongly coupled stochastic excitable elements, *Phys. Rev. E* **98**, 052303 (2018).
- [31] N. L. Neubarth, A. J. Emanuel, Y. Liu, M. W. Springel, A. Handler, Q. Zhang, B. P. Lehnert, C. Guo, L. L. Orefice, A. Abdelaziz *et al.*, Meissner corpuscles and their spatially intermingled afferents underlie gentle touch perception, *Science* **368**, 6497 (2020).
- [32] G. J. Gerling, L. Wan, B. U. Hoffman, Y. Wang, and E. A. Lumpkin, Computation predicts rapidly adapting mechanotransduction currents cannot account for tactile encoding in merkel cell-neurite complexes, *PLoS Comput. Biol.* **14**, e1006264 (2018).
- [33] J. Feng, J. Luo, P. Yang, J. Du, B. S. Kim, and H. Hu, Piezo2 channel—Merkel cell signaling modulates the conversion of touch to itch, *Science* **360**, 530 (2018).
- [34] R. W. Carr, J. E. Gregory, and U. Proske, Summation of responses of cat muscle spindles to combined static and dynamic fusimotor stimulation, *Brain Res.* **800**, 97 (1998).
- [35] J. B. Fallon, R. W. Carr, J. E. Gregory, and U. Proske, Summing responses of cat soleus muscle spindles to combined static and dynamic fusimotor stimulation, *Brain Res.* **888**, 348 (2001).
- [36] A. Borst and F. E. Theunissen, Information theory and neural coding, *Nat. Neurosci.* **2**, 947 (1999).
- [37] F. Rieke, D. Warland, R. D. R. Van Steveninck, W. S. Bialek *et al.*, *Spikes: Exploring the Neural Code* (MIT Press, Cambridge, MA, 1999), Vol. 7.
- [38] S. O. Voronenko and B. Lindner, Improved lower bound for the mutual information between signal and neural spike count, *Biol. Cybern.* **112**, 523 (2018).
- [39] N. Brunel and J.-P. Nadal, Mutual information, fisher information, and population coding, *Neural Comput.* **10**, 1731 (1998).
- [40] B. C. Ross, Mutual information between discrete and continuous data sets, *PLoS ONE* **9**, e87357 (2014).
- [41] T. E. Harris, *The Rtheory of Branching Process* (Rand Corporation, Berlin, Gottingen, Heidelberg, 1964).
- [42] M. Drmota, *Random Trees: An Interplay between Combinatorics and Probability* (Springer Science & Business Media, New York, 2009).
- [43] A. Khaledi-Nasab, Collective Dynamics of Excitable Tree Networks. Ph.D. thesis, Ohio University (2019).
- [44] A. Pikovsky, J. Kurths, M. Rosenblum, and J. Kurths, *Synchronization: A Universal Concept in Nonlinear Sciences* (Cambridge University Press, Cambridge, UK, 2003), Vol. 12.
- [45] D. Orr and B. Ermentrout, Synchronization of oscillators via active media, *Phys. Rev. E* **99**, 052218 (2019).
- [46] S. A. Wellnitz, D. R. Lesniak, G. J. Gerling, and E. A. Lumpkin, The regularity of sustained firing reveals two populations of slowly adapting touch receptors in mouse hairy skin, *J. Neurophysiol.* **103**, 3378 (2010).
- [47] R. Banks, M. Hulliger, and K. Scheepstra, Correlated histological and physiological observations on a case of common sensory output and motor input of the bag 1 fibre and a chain fibre in a cat tenuissimus spindle, *J. Anat.* **193**, 373 (1998).
- [48] M. Shamir and H. Sompolinsky, Implications of neuronal diversity on population coding, *Neural Comput.* **18**, 1951 (2006).
- [49] E. Hunsberger, M. Scott, and C. Eliasmith, The competing benefits of noise and heterogeneity in neural coding, *Neural Comput.* **26**, 1600 (2014).
- [50] M. J. Chacron, A. Longtin, M. St-Hilaire, and L. Maler, Suprathreshold Stochastic Firing Dynamics with Memory in P-Type Electroreceptors, *Phys. Rev. Lett.* **85**, 1576 (2000).
- [51] Y. Fukami, Interaction of impulse activities originating from individual golgi tendon organs innervated by branches of a single axon, *J. Physiol.* **298**, 483 (1980).
- [52] S. Roatta, U. Windhorst, M. Ljubisavljevic, H. Johansson, and M. Passatore, Sympathetic modulation of muscle spindle afferent sensitivity to stretch in rabbit jaw closing muscles, *J. Physiol.* **540**, 237 (2002).
- [53] B. Frankenhaeuser and A. Huxley, The action potential in the myelinated nerve fibre of xenopus laevis as computed on the basis of voltage clamp data, *J. Physiol.* **171**, 302 (1964).